Experimental Evidence for the Curve Crossing Mechanism for Collisional Excitation in keV $N_2^{+\bullet}$/He Collisions by Emission Spectroscopy

Clement Poon and Paul M. Mayer*

Department of Chemistry, University of Ottawa, 10 Marie-Curie, Ottawa, Ontario, Canada K1N 6N5

Received: October 14, 2006; In Final Form: December 6, 2006

Collision-induced emission (CIE) experiments were carried out by coupling a spectrograph and charge-coupled device detector (CCD) to a commercial analytical mass spectrometer. An Einzel lens and a deceleration−reacceleration lens assembly as described in the current article were installed in the mass spectrometer to allow for the deceleration of the ions before collision. Collision-induced emission spectra of $N_2^{+\bullet}$/He collisions at lab frame collision energies from 2 to 8 keV were obtained from 190−1020 nm. The emissions were assigned to the $\Delta v = +2, +1, 0, -1, -2$ vibrational transition progression in the $N_2^{+\bullet}$ B $^2\Sigma_u^+ \rightarrow$ X $^2\Sigma_g^+$ electronic transition as well as some atomic lines from the fragments N^+, $N^\bullet$ and the target gas He. $N_2^{+\bullet}$ A $^2\Pi_u \rightarrow$ X $^2\Sigma_g^+$ emission was also observed but was very weak due to the long lifetime of the A $^2\Pi_u$ state. The relative intensities of the $N_2^{+\bullet}$, N, and N^+ emissions are independent of the ion translational energy within the studied energy range. This observation supports the curve-crossing mechanism for collisional excitation, suggesting that a complicated sequence of curve-crossings takes place upon collisional activation.

1. Introduction

Collision-induced dissociation (CID) plays a very important role in structural determinations by mass spectrometry.[1−4] However, in spite of the enormous practical importance of CID, the mechanisms involved in the energy transfer in keV collisions remain poorly understood. A number of possible mechanisms for the energy transfer from translational to internal modes in ion-target gas collisions have been described.[5,6] Among these mechanisms, vertical transitions and curve crossings are deemed the most likely for high-energy collisions such as those in the keV range.

The vertical excitation mechanism is basically the same as that known for photoexcitation. Stated in the Franck−Condon principle,[7,8] because the nuclei are so much more massive than the electrons, an electronic transition takes place faster than the nuclei can respond. Therefore, the most probable transition is the one at which the initial state and the excited-state have the most similar geometries (i.e., with the largest overlap integral between the two wavefunctions). As a result, vertical excitation is expected to be important only at short interaction times (10^{-14} or less). In most MS/MS experiments with present-day instrumentation, interaction times tend to be longer than 10^{-14} s, especially for molecular masses that are higher than a few hundred mass units.[6] However, it may be important for very light precursor ions (e.g., below 50 mass units) in the keV collision energy range and is known to be so for some diatomic ions.[1]

The curve crossing mechanism is most frequently credited for electronic transitions in the collisional activation of polyatomic species, wherein a net transition occurs at an avoided crossing along the ion-target coordinate (see Figure 1).[6,9,10] As the collision partners get closer to each other, the energy of the collision complex increases along the adiabatic curve of the ground state. At a point where this surface is close to those of higher excited states, the surface may cross through nonadiabatic interactions that bring about radiationless transitions from the ground to electronic excited states of the collision complex. When the collision partners then separate, these excited states correlate with the excited states of the reactants. De Froidmont et al.[11] carried out a theoretical study of the keV collisions of H_3^+ with He. They concluded from their adiabatic potential energy curves that a very complicated sequence of non-adiabatic interactions is involved in transforming kinetic energy into electronic energy. In a two-state interaction, the strength of the nonadiabatic coupling can be measured by the Massey parameter (ξ) which is a velocity-dependent quantity

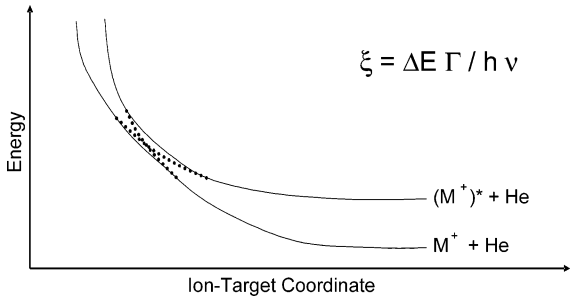

Figure 1. Simplified diagram illustrating curve-crossings during ion-target collisions. The behavior of the excited states is drawn as a single entity. The strength of the nonadiabatic coupling can be measured by the Massey parameter, ξ. ΔE is the smallest energy gap between two adiabatic states, Γ is the width of the nonadiabatic interaction region, and v is the classical nuclear velocity.

$$\xi = \Delta E \Gamma / \hbar v$$

where ΔE is the smallest energy gap between two adiabatic states, Γ is the width of the nonadiabatic interaction region, and v is the classical nuclear velocity. A small value of ξ ($\xi \ll 1$) indicates a strong propensity to follow the diabatic curves (i.e., to retain its electronic configuration). A large value of ξ ($\xi \gg 1$) indicates that the system behaves adiabatically, following

* Corresponding author. Tel: (613) 562-5800 ext. 6038. Fax: (613) 562-5170. E-mail: pmmayer@uottawa.ca.

10.1021/jp066755v CCC: $37.00
Published on Web 01/18/2007

the noncrossing curves. For intermediate values of ξ, a branching takes place with a probability given by the Landau−Zener formula

$$P = \exp[-\pi\xi/4]$$

In our study, we use the technique of collision-induced emission (CIE)[12] to probe the collision event in CID more thoroughly. This technique has been intensely used, especially on the study of N_2[13−32] and CO_2.[33−40] It has also been used previously in our lab to study ion-target gas collisions at 8 kV.[32,40,41] Due to the difference in the nature of the two excitation models presented above, they would lead to different results with respect to the emission intensities when collisions are performed at different ion translational energies. According to the vertical transition model, electronic transitions to various excited states take place simultaneously and in competition with each other. Higher ion translational energy (i.e., higher ion velocity) should therefore favor higher-energy transitions. As a result, as collision energy increases, we would expect to see relatively stronger emissions from species formed at higher internal energies (such as excited-state fragments). On the other hand, if the curve-crossing mechanism is dominant, transitions occur at a few curve-crossing points and may then be followed by a complicated sequence of nonadiabatic interactions. As the Massey parameter indicates, higher ion translational energy will increase the probability that the system will follow the diabatic curves, forming excited-state species. As such, the same excited-state species will be formed at all ion translational energies, and the distribution of these species will be constant.

There have been several studies in which the emission spectrum from keV projectile-N_2 target collisions were obtained [13−18,24,26−28,30,31] but relatively few in which $N_2^{+\bullet}$ was the projectile.[19,29,32] Bregman-Reisler et al.[29] studied the relative band intensities of the $\Delta v = -1$ sequence of the $N_2^{+\bullet}$ $B^2\Sigma_u^+ \rightarrow X^2\Sigma_g^+$ emissions at collisions of $0.3 - 5$ keV $N_2^{+\bullet}$ ions with He. At ion velocities over 1.2×10^{-5} m/s (i.e., 2 keV), the relative populations of the vibrational levels in the upper state were found to be independent of velocity. Many authors invoked a Franck−Condon picture on the grounds that the very brief transition time does not allow the nuclei to vibrate and concluded that at high projectile-ion velocities, the vibrational-energy distribution of the collision products is well described by the application of the Franck−Condon principle to the excitation process.[14,16,27,29,30,35,36,42] In the present article, we report our CIE results from $N_2^{+\bullet}$/He collisions (as a function of projectile ion translational energy) over a broader range of wavelengths ($190 - 1020$ nm) than has previously been reported (typically spectra have been reported for wavelengths ranging from 380−392 nm[13,15] to 180−850 nm[21]). By observing the emissions from the fragments resulting from higher internal energy $N_2^{+\bullet}$ ions, we are probing excited states that involve energy depositions upward of 28 eV, as compared to only ~3 eV for $N_2^{+\cdot}$ emissions.

2. Experimental Methods

The CIE experiments were performed on a modified VG ZAB mass spectrometer. The original, double focusing instrument[43,44] and the added third field-free region (3FFR) with an experimental zone designed for this work have been described previously.[32] An expanded view of the 3FFR is shown in Figure 2. The 3FFR consists of a 1 m long box differentially pumped by two six-inch diffusion pumps and ending in a second electrostatic analyzer. A deceleration-reacceleration lens assembly (see below) with a collision cell is mounted on the two rails underneath the fused silica window (Optikon WU-25). Collisions were performed in the collision cell, and emissions from the excited ion beam and target gas were directly observed. The time window of observation ranges from 0.00 to 0.05 μs for 8 keV $N_2^{+\bullet}$ to 0.00−0.09 μs for 2 keV $N_2^{+\bullet}$, depending on the translational energy of the projectile ion.

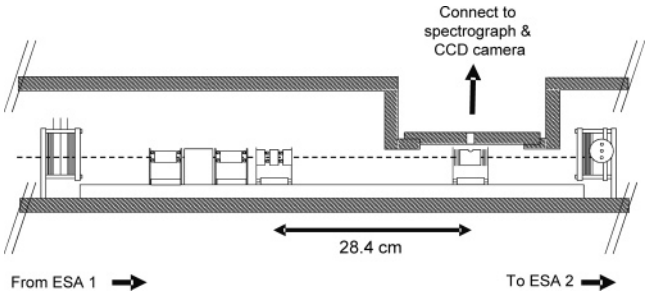

Figure 2. Expanded view (drawn-to-scale) of the inside of the third field-free region, including the location of the Einzel lens and the deceleration−reacceleration collision cell assembly. To ensure mechanical alignment, two optically correct rails run along the bottom of the box, allowing collision cells and other experimental hardware to be precisely located in the ion beam path. Two collision cells and a repeller electrode have already been mounted on the rails and are used for typical tandem mass spectrometry experiments.

A spectrograph (Acton SpectraPro 275, 27.5 focal length, 1200 g mm^{-1} holographic grating) and a thermoelectrically cooled charge-coupled device (CCD) (Andor DV401-UV, front-illuminated with UV coating) cooled to −35 °C were used to monitor the emission spectra. The experiments were performed with helium collision gas at a pressure which reduces the pre-cell ion flux by 10% (i.e., single collision conditions). The exit slit of the monochromator was set to 3 mm to maximize emission signal intensity resulting in a spectral resolution of 8.5 nm (full width at half-height for atomic lines). Optical emissions from 190 to 1020 nm were recorded by the Andor MCD 2.63.1.8 program and were recorded in 14 separate segments, each being 70 nm wide. Two accumulations of 15 min were collected for each segment at full vertical binning reading mode and each of the 14 segments was background subtracted. Background spectra were collected prior to the signal acquisition at exactly the same conditions except without an ion beam. Spectral spikes resulting from cosmic rays were removed digitally by the program. Horizontal binning was performed manually in the ASCII file by combining data from every 10 pixel columns and the overlapping spectrum at the end of each window was averaged.

2.1. Construction of a Deceleration−Reacceleration Lens Assembly. A schematic diagram of the deceleration-reacceleration lens assembly is shown in Figure 3a. The collision chamber is a 16-mm ID cylindrical tube with a 6-mm diameter circular hole drilled at the top covered by a fused silica (UV grade) window (Edmund Optics). On each side of the collision cell are six circular plates and rectangular ground plate separated by 2-mm spacers. A number of resistors create a gradual voltage drop before the collision cell and a gradual voltage gain after the collision cell when a voltage is applied to the collision cell. The net result is a deceleration−reacceleration lens assembly. An illustration of the change in kinetic energy across the lens is shown in Figure 3a.

Ion trajectory modeling with the SIMION 6.0 program[45] showed that a high deceleration voltage applied to the cell (such as 7900 V for an 8 keV ion beam) resulted in a very scattered ion beam (Figure 3b). However, with the installation of an Einzel lens to focus the ion beam before it enters the deceleration lens, ion scattering is significantly reduced (Figure 3b). As a result,

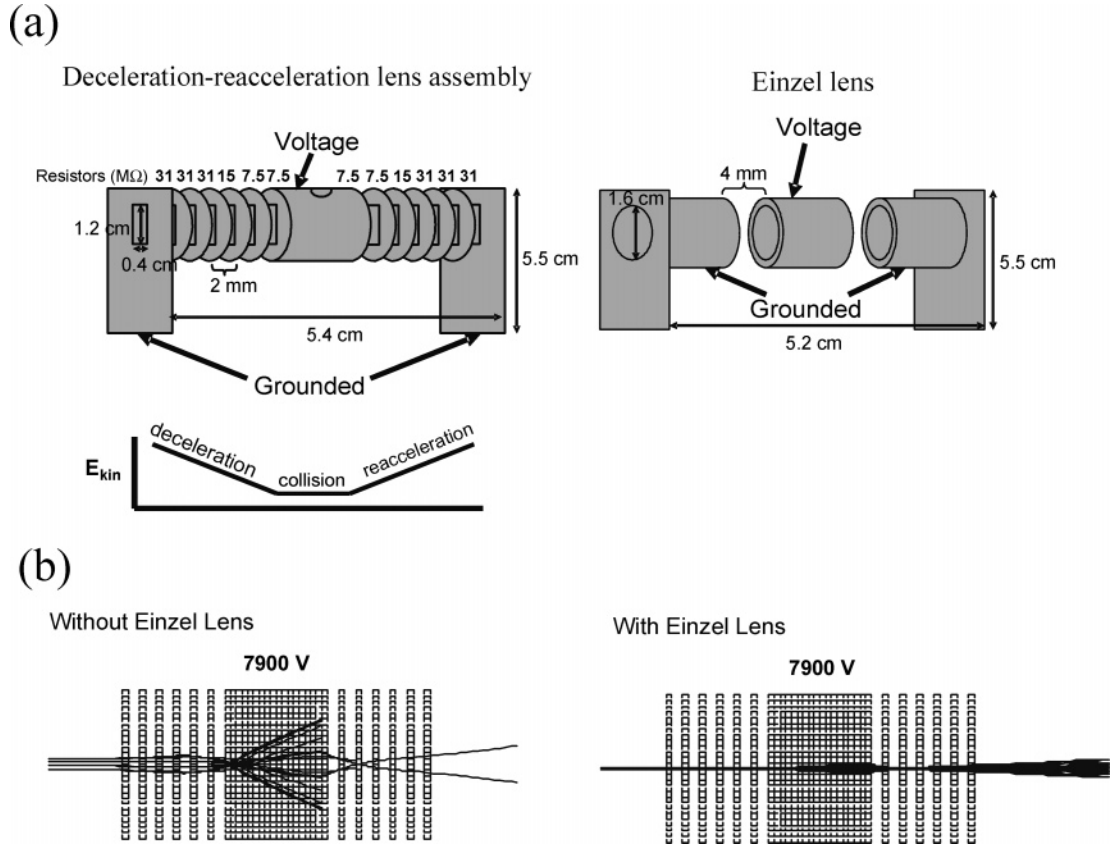

Figure 3. (a) Dimensions of the deceleration−reacceleration lens assembly and Einzel lens with a schematic diagram demonstrating the behavior of the ion kinetic energy in the assembly. The collision chamber is a 16-mm ID aluminum cylindrical tube with a thickness of 4.7 mm and a length of 16 mm. A 6-mm diameter circular hole is drilled at the top of the tube and covered by a fused silica (UV grade) window (Edmund Optics, 10 mm diameter, 1 mm thickness) for photon transmission. On each side of the collision cell are six circular plates made of brass (2.54 cm diameter with a slit of 12 × 4 mm) and an aluminum rectangular ground plate (55 × 30 mm with a slit of 12 × 4 mm). The plates are separated by 2-mm ceramic spacers and are mounted on 4 ceramic rods. The whole assembly is mounted on a stainless steel plate which is subsequently mounted onto the two parallel rails running along the bottom of the 3FFR. A number of 33 MΩ and 15 MΩ resistors (Electrosonics VR 37J 33M and VR 37J 15M) create a gradient before and after the collision cell. The Einzel lens consists of three 16-mm ID aluminum cylindrical tubes with a thickness of 4.7 mm and a length of 14 mm. On each end of the Einzel lens is a rectangular aluminum ground plate (55 × 30 mm with a circular opening of 16-mm diameter). The cylindrical tubes are separated by 4-mm spacers and the whole assembly is connected by four ceramic rods and mounted on a stainless steel plate on the two optically correct rails. (b) SIMION modeling of the behavior of an 8 keV ion beam in the deceleration-reacceleration lens assembly with an applied voltage of 7900 V, with and without the use of an Einzel lens.

an Einzel lens was installed at 28.4 cm before the collision cell that can be used to focus the ion beam when needed (see Figure 2).

2.2. Characterization of the Deceleration−Reacceleration Lens. To characterize the deceleration−reacceleration lens, the beam-resolving slits of the VG ZAB were set for high resolution and an 8 keV $N_2^{+\bullet}$ beam was passed through the lens. The intensity, energy and energy spread (full peak width at half-height) of the beam were measured as a function of applied voltage (Figure S1). Ions can be decelerated to 3 keV without much intensity loss (Figure S1a). The reaccelerated main beam energy is within 0.8% of the original 8 keV (Figure S1b). This small difference can be considered insignificant when comparing ion energy difference in the range of keV. The energy spread of the reaccelerated beam does not change significantly with the use of the lens (Figure S1c).

To correlate ion translational energies with applied voltage, a simple metastable ion experiment was performed (Figure S2). When a voltage is applied to the collision cell, daughter ions formed in the cell will have a different translational energy than those formed outside the cell. By measuring the energy shift for the peaks from two competing dissociations of a proton-bound pair, a correlation plot of ion translational energy vs applied voltage was obtained with a slope close to −1 ($y = -1.01x + 8027$, $R^2 = 1.000$; Figure S2c).

Two ways of decelerating the ions to the desired ion translational energy were compared. One way is to decelerate an 8 keV ion beam to the desired ion translational energy with the deceleration−acceleration lens only (Figure S3a). The other way is to use a lower accelerating voltage on the VG ZAB ion source and then fine-tune to the desired ion translational energy with the deceleration lens (Figure S3b). The second method resulted in less intensity loss and appears to be better for obtaining ions at low ion translational energy.

2.3. $N_2^{+\bullet}$ Ion Beams. The $N_2^{+\bullet}$ ion beam was generated by electron impact (EI) on N_2 using ∼80 eV electrons. With an electron energy of 59 eV, the $N_2^{+\bullet}$ ion population can be up to 60% $A^2$and about 14% $B^2\Sigma_u^+$ state (the amount of $C^2\Sigma_u^+$ state is almost negligible, <0.5%).[46] The lifetimes of the B and C states are 6×10^{-8} s and 1×10^{-7} s respectively,[47−49] whereas the time required for the ions to reach the collision chamber ranges from 14 to 27 μs, depending on the accelerating voltage. Therefore, ions that are formed initially in the B and C states will undergo spontaneous radiative decay to the ground state before arriving at the collision cell. The $A^2\prod_u$ state of $N_2^{+\bullet}$ has a lifetime of 8−15 μs, depending on the vibrational level.[50]

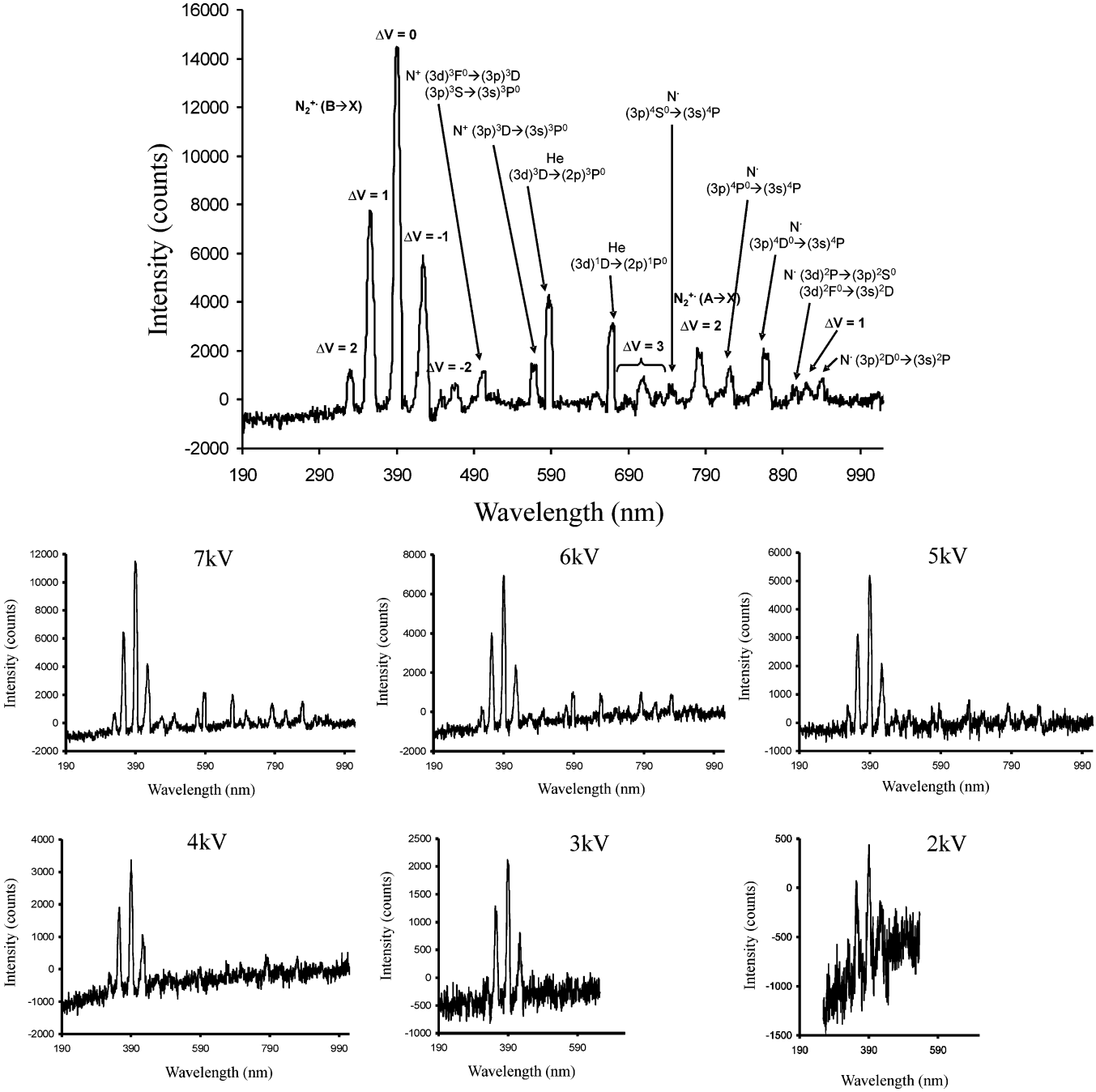

Figure 4. Collision-induced emission spectra (190−1020 nm) of $N_2^{+\bullet}$/He collisions at (a) 8 keV and (b) at other projectile ion translational energies. All ion translational energies were obtained by varying the source accelerating voltage, except at 2 kV which was obtained from a 3 keV ion beam with +1 kV applied to the collision cell. Spectra are normalized to the ion flux at 8 keV. Collision gas pressure corresponded to 90% ion beam transmission.

Therefore, considerable $N_2^{+\bullet}$ A $^2\Pi_u$ may be involved in the collision events. However, if $N_2^{+\bullet}$ A $^2\Pi_u$ was a significant fraction of the ion flux, $N_2^{+\bullet}$ A $^2\Pi_u \rightarrow$ X $^2\Sigma_g^+$ emissions might be expected to be observed in the absence of target gas. Since it could not be detected without the presence of target gas, we concluded that $N_2^{+\bullet}$ A $^2\Pi_u$ makes up a negligible fraction of the ion beam.

3. Results and Discussion

The emission spectra over the wavelength range of 190−1020 nm obtained from $N_2^{+\bullet}$/He collisions at different projectile ion translational energies are presented in Figure 4a. A prominent feature at low wavelength is the $\Delta v = +2, +1, 0, -1, -2$ vibrational transition progression in the $N_2^{+\bullet}$ B $^2\Sigma_u^+ \rightarrow$ X $^2\Sigma_g^+$ electronic transition.[51] The A $^2\Pi_u \rightarrow$ X $^2\Sigma_g^+$ electronic transition ($\Delta v = +3, +2, +1$) is also observed but the peaks are weaker due to the longer lifetime of the A $^2\Pi_u$ state. The other peaks arise from the emissions of the excited N^+ and $N^\bullet$ fragments, resulting from the dissociation of $N_2^{+\bullet}$ with higher internal energies. Emissions from the helium target gas are also observed. A summary of the peak and transition assignments is presented in Table 1.

As shown in Figure 4b, the relative intensities of the spectral peaks appear to be constant with changing ion translational energy. The only difference is the decrease in signal-to-noise ratio with decreasing ion translational energy. To better show these observations, the absolute emission intensities of $N_2^{+\bullet}$, N^+, and $N^\bullet$ at various collision energies vs that at 8 keV is

TABLE 1: Observed Emissions in Figure 4 and Their Corresponding Radiative Lifetimes

transition			τ (ns)[a]	λ (nm)	refs
$N_2^{+\bullet}$	$B\ ^2\Sigma_u^+ \rightarrow X\ ^2\Sigma_g^+$	$\Delta v = +2$	~60	331	47,48,51
		+1		356	
		0		390	
		−1		425	
		−2		467	
$N_2^{+\bullet}$	$A\ ^2\Pi_u \rightarrow X\ ^2\Sigma g^+$	$\Delta v = +3$	8000−15000	691	50,51
		+3		710	
		+3		730	
		+2		785	
		+1		922	
N^+	$(3d)\ ^3F^0 \rightarrow (3p)\ ^3D$		8	503	53,54
	$(3p)\ ^3S \rightarrow (3s)\ ^3P^0$		13	503	
	$(3p)\ ^3D \rightarrow (3s)\ ^3P^0$		18	570	
N	$(3p)\ ^4S^0 \rightarrow (3s)\ ^4P$		31	748	53,54
	$(3p)\ ^4P^0 \rightarrow (3s)\ ^4P$		44	822	
	$(3p)\ ^4D^0 \rightarrow (3s)\ ^4P$		52	872	
	$(3d)\ ^2P \rightarrow (3p)\ ^2S^0$		39	906	
	$(3p)\ ^2F^0 \rightarrow (3s)\ ^2D$		37	906	
	$(3p)\ ^2D^0 \rightarrow (3s)\ ^2P$		46	941	
He	$(3d)\ ^3D \rightarrow (2p)\ ^3P^0$		14	590	53,54
	$(3d)\ ^1D \rightarrow (2p)\ ^1P^0$		16	671	

[a] Lifetimes from refs 47, 48, 50, and 53.

plotted in Figure 5a. The plotted values have been normalized to the flux of the 8 keV $N_2^{+\bullet}$ beam to correct for any difference in ion flux between experiments. The $A\ ^2\Pi_u \rightarrow X\ ^2\Sigma_g^+$ peaks are not plotted since they are weak and their assignment remains uncertain. Figure 5a clearly shows that the absolute emission intensities decrease with decreasing ion translational energy. A similar plot is made for the relative intensities (Figure 5b). All of the points fall along the $y = x$ line, indicating that relative intensities from $N_2^{+\bullet}$, N^+, and $N^\bullet$ do not change with ion translational energy (for an expanded view of the N^+ and $N^\bullet$ emission region of Figure 5b, see Figure S4). We can therefore conclude from these results that as the ion translational energy decreases, the population in the excited states decreases, but the relative population distribution in these states remains constant.

A number of possible sources of error have been considered. It is possible that ion scattering could be responsible for the decrease in absolute intensities at lower translational energies. A worst case scenario has the collision occurring at the beginning of the collision cell. The projectile ions need to be scattered by over 20° from the ion beam in order to miss the optical window. Based on the absolute differential cross sections for direct scattering of O^+ by He,[52] even at translational energies as low as 1.5 keV, scattering decreases by 3 orders of magnitude from 0.24° to 4.67° laboratory angle. Therefore, scattering over 20° is negligible. Similarly, in order for ions to be scattered at a large enough angle so that they cannot exit the collision cell (and thus not be transmitted by the electrostatic analyzer), the scattering angle needs to be over 3.5°. From the differential cross sections of O^+/He collisions, over 98% of the ions would pass through the exit slit at 1.5 keV ion translational energy. Therefore, we feel it is valid to use ion flux to normalize the absolute intensity and 10% beam reduction as a reference point for collision conditions at different ion translational energies. The lifetimes of different emitting species also need to be considered, since we are only observing a portion of the emission from the excited-state species. Again, taking collisions at the beginning of the cell as the worst case scenario, Figure 5c shows the plot of the relative intensities after radiative lifetimes have been taken into consideration (by calculating the fraction of the total emission that occurs under the window

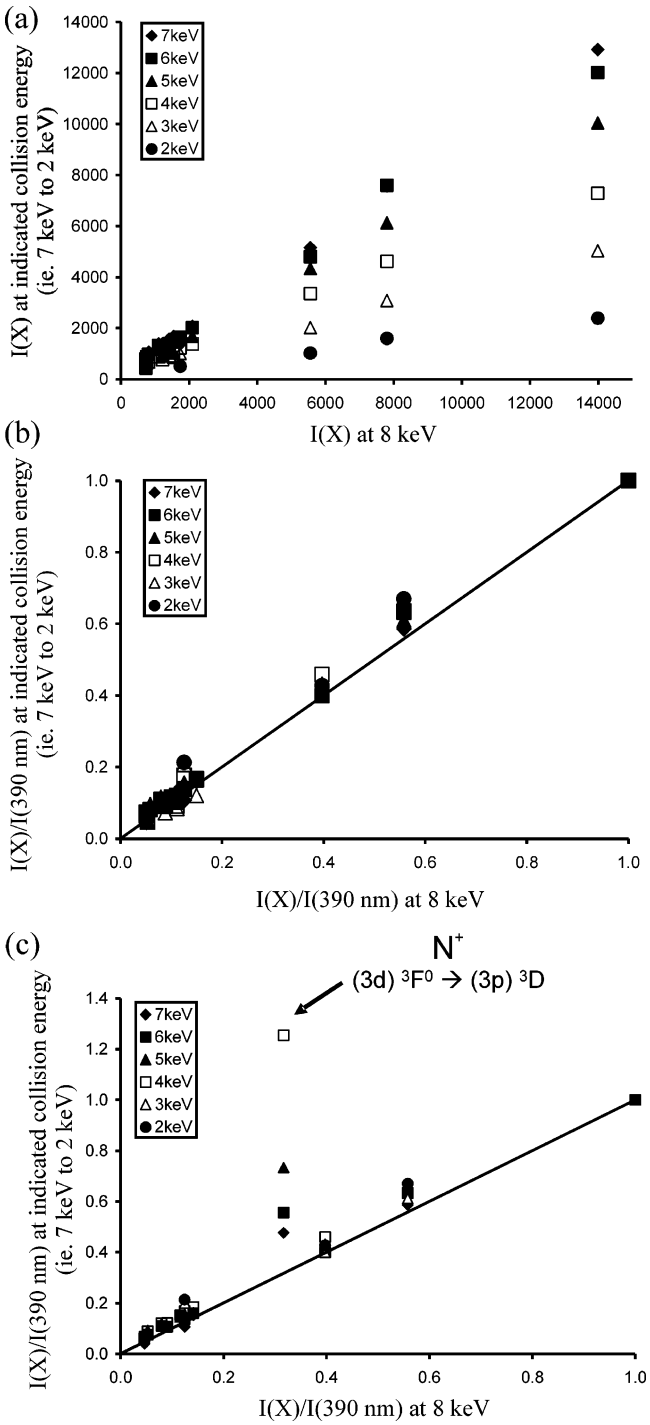

Figure 5. Plot of (a) the absolute emission intensities, (b) the relative emission intensities, and (c) the lifetime-corrected relative emission intensities of $N_2^{+\bullet}$, N^+, and $N^\bullet$ at various ion translational energies vs those at 8 keV. $I(X)$ represents the intensity of $N_2^{+\bullet}$, N^+, and $N^\bullet$ and I(390 nm) the intensity of the $B\ ^2\Sigma_u^+ \rightarrow X\ ^2\Sigma_g^+B$ ($\Delta v = 0$) transition. All ion translational energies were obtained by varying the source accelerating voltage, except at 2 keV which was obtained from a 3 keV ion beam with +1 kV applied to the collision cell. Spectra are normalized to the ion flux at 8 keV. Collision gas pressure corresponded to 90% ion beam transmission. Uncertainties, based on replicate measurements, are represented by the size of the symbols in the figures.

leading to the spectrograph and correcting the peak intensity accordingly). It was found that only one emitting state is affected due to its significantly short lifetime (~8 ns for N^+ $(3d)\ ^3F^0 \rightarrow (3p)\ ^3D$). However, there is no reason for this one particular excited-state species to be preferentially generated at high

translational energy indicating that the above treatment is indeed an extreme correction for radiative lifetime and that the vast majority of collision events take place under the window. Therefore, for N_2^+/He collisions, lifetime constraints do not affect our previously stated conclusions. The intensities of the emissions from the target gas cannot be directly compared with those from the projectile ions or fragments since the spatial distribution of collisions across the collision cell is unknown.

According to the vertical transition model in which the electronic transitions take place simultaneously and in competition with each other, we would expect the higher excited states to be less populated as collision energy decreases; thus, emissions from the fragments were expected to decrease with decreasing collision energy. However, from our results, this is obviously not the case, and thus a different explanation needs to be invoked. If we apply the curve-crossing model, as ion translational energy (i.e., ion velocity) increases, the Massey parameter indicates a higher probability to cross to higher-excited states. The intricate succession of nonadiabatic interactions that follows can then lead to a consistent population distribution in the excited states. It would also suggest that, when the ion translational energy is changed, the observed emission always comes from excited states arising from the same crossing points.

4. Conclusions

The excited-state species formed as a result of high keV $N_2^{+\bullet}$/He collisions were probed by collision-induced emission spectroscopy. The relative population of electronically excited $N_2^{+\bullet}$, N, and N^+ states remains constant as the collision energy is increased from 2 to 8 keV. This result cannot be explained by a purely vertical transition model which subsequently leads to emission. However, it agrees with the curve-crossing mechanism in which a complicated sequence of curve-crossings are involved among the excited states prior to emission, leading to a lower overall population, but same relative population among the excited states, as collision energy decreases.

Acknowledgment. The authors thank the Natural Sciences and Engineering Research Council (NSERC) of Canada for continuing financial support. CP thanks NSERC for a postgraduate scholarship during the tenure of which this work is completed.

Supporting Information Available: Additional figures (Figures S1−S4). This material is available free of charge via the Internet at http://pubs.acs.org.

References and Notes

(1) Cooks, R. G. *Collision Spectroscopy*; Plenum Press: New York, 1978.
(2) Holmes, J. L. *Org. Mass Spectrom.* **1985**, *20*, 169.
(3) Levsen, K.; Schwarz, H. *Mass Spectrom. Rev.* **1983**, *2*, 77.
(4) Todd, P. J.; McLafferty, F. W. *Tandem Mass Spectrometry*; Wiley-Interscience: New York, 1983.
(5) Durup, J. *Recent developments in mass spectrometry*; University of Tokyo Press: Tokyo, 1970.
(6) McLuckey, S. A. *J. Am. Soc. Mass Spectrom.* **1992**, *3*, 599.
(7) Condon, E. U. *Am. J. Phys.* **1947**, *15*, 366.
(8) Atkins, P. *Physical Chemistry*; W. H. Freeman and Company: New York, 1998.
(9) Reid, C. J. *Int. J. Mass Spectrom. Ion Processes* **1991**, *105*, 191.
(10) Reid, C. J. *Int. J. Mass Spectrom. Ion Processes* **1990**, *101*, 35.
(11) de Froidmont, Y.; Lorquet, A. J.; Lorquet, J. C. *J. Phys. Chem.* **1991**, *95*, 4220.
(12) Leventhal, J. J. *The emission of light from excited products of charge exchange reactions*; Academic Press: Orlando, FL, 1984; Vol. *3*.
(13) Moore, J. H.; Doering, J. P. *Phys. Rev.* **1968**, *174*, 178.
(14) Moore, J. H.; Doering, J. P. *Phys. Rev.* **1969**, *177*, 218.
(15) Moore, J. H.; Doering, J. P. *Phys. Rev.* **1969**, *182*, 176.
(16) Birely, J. H. *Phys. Rev. A* **1974**, *10*, 550.
(17) Zyl, B. V.; Gealy, M. W.; Neumann, H. *Phys. Rev. A* **1983**, *28*, 2141.
(18) Matsumoto, A.; Sano, T.; Iwai, T. *J. Phys. Soc. Jap.* **1983**, *52*, 1173.
(19) Doering, J. P. *Phys. Rev.* **1964**, *133*, A1537.
(20) Leventhal, J. J.; Earl, J. D.; Harris, H. H. *Phys. Rev. Lett.* **1975**, *35*, 719.
(21) Bearman, G. H.; Earl, J. D.; Pieper, R. J.; Harris, H. H.; Leventhal, J. J. *Phys. Rev. A* **1976**, *13*, 1734.
(22) Kelley, J. D.; Bearman, G. H.; Harris, H. H.; Leventhal, J. J. *Chem. Phys. Lett.* **1977**, *50*, 295.
(23) Kelley, J. D.; Bearman, G. H.; Harris, H. H.; Leventhal, J. J. *J. Chem. Phys.* **1978**, *68*, 3345.
(24) Bearman, G. H.; Leventhal, J. J. *Phys. Rev. A* **1978**, *17*, 80.
(25) Barrett, J. L.; Leventhal, J. J. *J. Chem. Phys.* **1979**, *71*, 4015.
(26) Ottinger, C.; Simonis, J. *Chem. Phys.* **1978**, *28*, 97.
(27) Obase, H.; Tsuji, M.; Nishimura, Y. *Chem. Phys. Lett.* **1984**, *105*, 214.
(28) Sekiya, H.; Tsuji, M.; Nishimura, Y. *J. Chem. Phys.* **1987**, *87*, 325.
(29) Bregman-Reisler, H.; Doering, J. P. *Phys. Rev. A* **1974**, *9*, 1152.
(30) Dowek, D.; Dhuicq, D.; Pommier, J.; Tuan, V. N.; Sidis, V.; Barat, M. *Phys. Rev. A* **1981**, *24*, 2445.
(31) Bachmann, R.; Ottinger, C.; Vilesov, a. F. *Chem. Phys. Lett.* **1993**, *203*, 314.
(32) Holmes, J. L.; Mayer, P. M.; Mommers, A. A. *Int. J. Mass Spectrom. Ion Processes* **1994**, *135*, 213.
(33) Parker, J. E.; Milner, R. G.; Robertson, A. M. *Int. J. Mass Spectrom. Ion Phys.* **1977**, *24*, 429.
(34) Haugh, M. J.; Birely, J. H. *J. Chem. Phys.* **1974**, *60*, 264.
(35) Bregman-Reisler, H.; Doering, J. P. *Chem. Phys. Lett.* **1974**, *27*, 199.
(36) Birely, J. H.; Johnson, P. A. *J. Chem. Phys.* **1975**, *62*, 4854.
(37) Bregman-Reisler, H.; Doering, J. P. *J. Chem. Phys.* **1975**, *62*, 3109.
(38) Moore, J. H. *J. Geophys. Res.* **1975**, *80*, 3727.
(39) Sim, W.; Haugh, M. *J. Chem. Phys.* **1976**, *65*, 1616.
(40) Holmes, J. L.; Mayer, P. M. *J. Mass Spectrom.* **1995**, *30*, 52.
(41) Holmes, J. L.; Mayer, P. M. *Eur. J. Mass Spectrom.* **1995**, *1*, 23.
(42) Birely, J. H. *Phys. Rev. A.* **1975**, *11*, 79.
(43) Holmes, J. L.; Mommers, A. A.; Terlouw, J. K.; Hop, C. E. C. A. *Int. J. Mass Spectrom. Ion Processes* **1986**, *68*, 249.
(44) Burgers, P. C.; Holmes, J. L.; Szulejko, J. E.; Mommers, A. A.; Terlouw, J. K. *Org. Mass Spectrom.* **1983**, *18*, 254.
(45) Dahl, D. A. *SIMION 3D Version 6.0*; Idaho National Engineering Laboratory: Idaho Falls, 1995.
(46) Maier, W. B. *J. Chem. Phys.* **1974**, *61*, 3459.
(47) Hesser, J. E.; Dressler, K. *J. Chem. Phys.* **1966**, *45*, 3149.
(48) Bennett, R. G.; Dalby, F. W. *J. Chem. Phys.* **1959**, *31*, 434.
(49) Fournier, P.; VandeRunstraat, C. A.; Govers, T. R.; Schopman, J.; deHeer, F. J.; Los, J. *Chem. Phys. Lett.* **1971**, *9*, 426.
(50) Holland, R. F.; Maier, W. B. *J. Chem. Phys.* **1972**, *56*, 5229.
(51) Lofthus, A.; Krupenie, P. H. *J. Phys. Chem. Ref. Data* **1977**, *6*, 113.
(52) Lindsay, B. G. *J. Geophys. Res.* **2004**, *109*, A08305.
(53) Wiese, W. L.; Smith, M. W.; Glennon, B. M. *Atomic Transition Probabilities*; National Bureau of Standards: Washington, DC, 1966; Vol. I.
(54) Bashkin, S.; Stoner, J. O. *Atomic energy levels & grotrian diagrams 1*; North-Holland Publishing Company: New York, 1975.